Material Properties of Ion Beam Coatings for use in Gravitational Wave Interferometers

Teal Pershing

August 2012

Abstract

Modern gravitational interferometers are limited in the most sensitive detection region by the thermal noise from test mass coatings applied to optimize the reflectance and optical absorption. Utilizing materials with low mechanical losses will reduce the Brownian thermal motion in these coatings and lower interferometer noise floors. Amorphous silicon coatings deposited through HWCVD and PECVD have yielded low mechanical losses, but ion beam-deposited (IBD) amorphous silicon coatings have yet to be characterized. We have measured the lowest mechanical loss of an amorphous silicon / silica bilayer coating deposited through IBD (Sample 16) at 295K as $\phi_{coating} = 3.9 \pm 0.4 \times 10^{-4}$. Assuming that the loss of silica alone is $\phi_{SiO_2} = 5 \times 10^{-5}$, the mechanical loss for the amorphous silicon layers in the bilayer coating was found to be $\phi_{a-Si} = 7.9 \times 10^{-4}$; the high mechanical loss of amorphous silicon shows that Sample 16's coating loss is limited by amorphous silicon at room temperature. The mechanical loss of a single layer amorphous silicon coating deposited using IBD (sample 10) was measured as a function of temperature and yielded a minimum mechanical loss of $\phi_{SiO_2} = 1.3 \pm 0.35 \times 10^{-5}$ at $T = 71$K.

Contents

Part I

Background

Since the prediction of gravitational waves by Einstein's general theory of Relativity, experimental verification of gravitational waves has been pursued for some time now. Gravitational wave detection would not only offer another piece of experimental evidence to reinforce Einstein's theory of gravitation, but the observation of a gravitational wave would open opportunities to additional gravitational experimentation and possibilities of imaging the universe through gravitational wave analysis. The search for gravitational waves continues for now, but groups around the world are working continuously to make the first detection.

Several different approaches to gravitional wave detection are in circulation amongst research groups around the world. The first attempts at gravitational wave detection utilized a large test mass cooled to near 0K; researchers hoped to observe a small perturbation of the test mass' length upon resonation by a passing gravitational wave[1]. However, most modern gravitational wave detectors utilize an interferometer approach. Interferometers in practice have larger bandwidths and lower sensitivities than bar detectors; however, the necessity for both optimal optical properties and minimal thermal conductance in gravitational interferometers presents several experimental challenges.

This paper presents a general overview into the investigation of interferometer mirror coating properties and features research on the properties of amorphous silicon coatings. Current gravitational interferometry noise challenges and modern techniques to minimize gravitational interferometry noise are presented. Experimental procedures for determining the mechanical loss of coatings as a function of frequency and sample temperature are described. The mechanical

losses of an amorphous silicon coating annealed at $450°C$ and an as-deposited amorphous silicon-silica bilayer coating are determined as a function of temperature and frequency, respectively. Both samples analyzed are deposited via ion beam-sputtering.

1   Sensitivity in Gravitational Interferometers

Fig. 1 shows the current sensitivity of Virgo, one of the world's leading gravitational interferometers, which is located near Pisa, Italy[2].
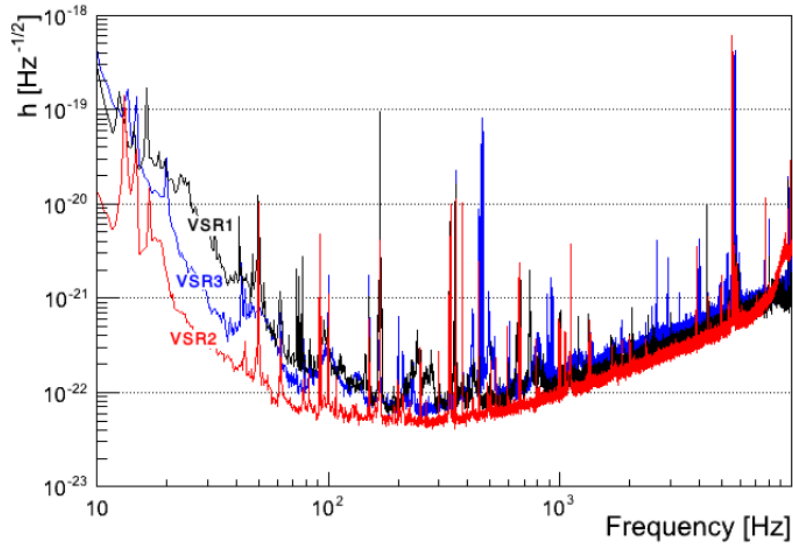

Figure 1: Sensitivities for several Virgo Science Runs (VSRs) with respect to signal frequency[2].

Sensitivity graphs for gravitational interferometers will commonly present the interferometer strain (units $Hz^{\frac{1}{2}}$) as a function of frequency. The strain measured in a gravitational interferometer is defined as

$$h \equiv \frac{\delta L}{L} \tag{1}$$

where δL is the net displacement of the test masses in a detector and L is the total interferometer arm length. At Virgo's maximum sensitivity for the VSRs in Fig. 1, strains of 10^{-22} are achievable. A strain on the order of 10^{-22} in the Virgo detector with arm length 3 km corresponds to detecting a test mass displacement on the order of 10^{-18} m. To give some length scale perspective, this interferometer sensitivity could successfully detect a change in test mass displacement on the order of one-thousandth of a proton diameter. To lower the region of maximum sensitivity for gravitational interferometers even further, the thermal noise throughout the interferometer, particularly on the test mass surfaces, must be minimized.

2   Interferometer Thermal Noise

The list of noise sources in gravitational interferometers is nearly endless, but several sources in particular greatly limit interferometer sensitivities. In the lower frequency regions, seismic noise and momentum transfer to the test masses from radiation pressure are the main noise sources. In higher frequency regions, shot noise resulting from the signal detector and the signal beam photons limit the detection range. Finally, in the region of maximum sensitivity, signal detection is limited by thermal noise and shot noise[2].

To reduce the thermal noise floor, leading interferometers in gravitational detection, including Virgo, LIGO, and GEO600, use test masses composed of amorphous silica (SiO_2). For example, in the Advanced LIGO design, two 40 kg silica pendulums are suspended using silica fibers with a diameter on the order of several microns as shown in Fig. 2 below. The silica fibers are used for

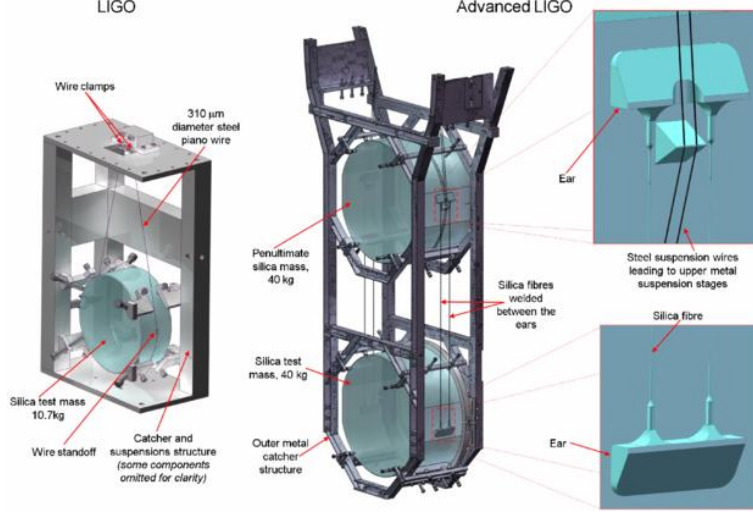filtering the seismic noise that limits low frequency detection.

Figure 2: Rendition of the future Advanced LIGO pendulum design. High-quality silica fibers are used to suspend the double pendulum system[3].

Unfortunately, the silica pendulums must also operate as mirrors in the gravitational interferometer. Since silica on its own has less than ideal optical properties for building signal power in the interferometer Fabry-Perot cavities, a coating consisting of alternating high and low refractive index bilayers is applied to the test masses and tailored to the desired reflectance. The presence of mirror coatings offers a unique experimental challenge: finding a coating that has the necessary optical properties while also having low energy dissipation.

3   Mirror coatings

Any coating applied to gravitational interferometer test masses must satisfy three main criteria: the coating must be highly reflective for use inside the Fabry-Perot cavities, the coating must demonstrate low optical absorption, and

the materials must have low energy dissipation for decreasing thermal noise. In particular, finding materials with a low energy dissipation is pivotal to minimizing gravitational interferometer noise; upon finding materials that will lower the noise floor in a gravitational interferometer, the optical properties can be further investigated and improved through techniques such as high and low refractive index multilayering, annealing, and material doping[4].

When considering the Brownian thermal motion in a mirror coating, the power spectral density function is generally used becuase it is proportional to the square of the thermal motion. The power spectral density (PSD) function describes the power dissipation exhibited in a sample for a particular input signal frequency. When deposited on a silica substrate, the PSD for a multilayer coating containing layers of silica can be approximated by setting the substrate and coating Poisson's ratios to $\sigma = \sigma' = 0$ to find[5]:

$$S_x(f)_{coating} = \frac{2k_B T}{\pi^2 f Y} \frac{d}{\omega_m^2} \left(\frac{Y'}{Y}\phi_\parallel + \frac{Y}{Y'}\phi_\perp \right) \propto X^2 \qquad (2)$$

where Y and Y' are the Young's modulus of the substrate and coating, d is the coating thickness, ω_m is the laser beam radius on the coating surface, X is the thermal motion in the coating, and $\phi_\parallel$ and $\phi_\perp$ are directional mechanical loss factors for the coating that are calculated using the individual mechanical losses of each coating layer material. From this equation, there are several possible strategies to lowering the coating's thermal motion, including: minimizing the mechanical loss of the coating materials, increasing the laser beam radius, reducing the overall sample thickness, and lowering the coating temperature.

3.1 Mechanical Loss

The mechanical loss of a material is important to characterizing a material as a candidate for gravitational interferometery. To define the mechanical loss of a

material, consider a large sample of some material. Assume that some oscillating stress σ is applied to the sample, represented as

$$\sigma(t) = \sigma_0 e^{i\omega t}.$$

Upon exposure to the stress, the material should respond with an oscillating strain ϵ. However, in non-ideal systems, the response of the material will lag behind the stress by some phase factor ϕ, leading to a strain represented by

$$\epsilon(t) = \epsilon_0 e^{i(\omega t - \phi)}$$

where ϕ is defined as the *loss angle* (or *mechanical loss*) of the material. Through some manipulation[12], the mechanical loss can also be defined in terms of the stress energy dissipated per cycle in the sample and the total energy stored in the sample as

$$\phi \equiv \frac{E_{lost/cycle}}{2\pi E_{stored}} \ . \tag{3}$$

The lower the mechanical loss factor, the lower the ratio of energy dissipated per cycle to energy stored; this is the desired material property for lowering coating thermal noise in interferometers.

Furthermore, the mechanical loss can be written as the inverse of a quality factor, where

$$\phi = \frac{\Delta f}{f_0} \tag{4}$$

where f_0 is the resonance frequency of the material sample and Δf is the full-width at half-maximum (FWHM) for the sample's resonant peak.

9

3.2 Coating Material Candidates

There are several materials that are commonly utilized and researched for coating applications in gravitational interferometers. Although the optical properties are not ideal, coatings that utilize silica in a multilayer setup are researched for silica's low mechanical loss at room temperatures. Tantala (Ta_2O_5) is also a common material found in test mass coatings; although other materials have lower mechanical losses, tantala also has the desired optical properties for interferometry purposes[6, 7]. The physical reason still remains unclear, but tantala's mechanical loss can also be reduced through the doping of titania (TiO_2), making the optimization of doped tantala's optical and thermal properties an active area of research. Currently, most modern gravatitional interferometers employ the use of titania-doped tantala / silica multilayer coatings, where each layer has and optical thickness of $\frac{\lambda}{4}$ for maximum reflectance.

Another potentially exciting coating material for gravitational interferometers is amorphous silicon $(a - Si)$. Research conducted at the Naval Research Laboratory in Washington, D.C. has measured mechanical loss factors for hydrogenated amorphous silicon prepared through hot wire chemical vapor deposition (HWCVD) on the order of 3×10^{-7} at $8 - 13$K, corresponding to energy dissipations several orders of magnitude lower than any other recorded amorphous solid[8]. Additionally, mechanical loss measurements are yet to be performed on an amorphous silicon coating deposited through ion-beam sputtering (IBS), leaving opportunity for further reductions in the energy dissipation and improvement in the reflective properties of amorphous silicon using IBS.

4 Cryogenics

Operation at near-zero temperatures is another option being considered for reducing interferometer thermal noise. Although a cost and resource-effective way of cooling the test masses would have to be produced, low operating temperatures provided by cryogenics could provide the sensitivity improvement necessary to successfully detect a gravitational wave. Operating at low temperatures also nearly eliminates the effects of thermoelastic loss, an energy dissipation effect resulting from thermal gradients in a material[9]. Once in operation, the KAGRA gravitational interferometer in Japan plans to use cryogenically-cooled test masses made from sapphire to surpass the sensitivities of current leading gravitational interferometers such as LIGO, Virgo, and GEO600[10].

A serious problem with the utilization of silica test masses is silica materials cannot be effectively used for cryogenic gravitational interferometry. Silica has a broad mechanical loss peak at ˜40K, so interferometer operation near liquid helium temperatures would result in a large mechanical loss that would negate any benefit to cooling the test masses. For cryogenic interferometry, crystalline silicon and sapphire are currently the leading candidates for test mass material choice. Crystalline silicon has a narrow mechanical loss peak at ˜25K; however, since liquid helium temperatures are˜4K, crystalline silicon test masses could be operated at a temperature beyond the mechanical loss peak and help to lower the interferometer's thermal noise.

Part II

Methods

This section will present a summary of the entire experimental procedure used to find the mechanical loss of coatings applied to cantilever samples. Theoretical concepts necessary to complete a mechanical loss analysis are described. Experimental preparation required (temperature control, pressure regulation, sample preparation, etc.) to perform measurements is also presented.

5   Experimental overview

Mechanical loss measurements are first performed on an uncoated cantilever at room temperature as a function of resonant frequency. The cantilever is clamped into the inside of a cryostat as shown in Fig. 3.

The cryostat is then sealed and evacuated to approximately 1×10^{-6} mbar. The mechanical loss of the cantilever is measured for all observable resonant frequencies at room temperature using a high-voltage drive plate for excitation and a ring-down technique described in sec. 6.1.1. Three trials of mechanical loss measurements are completed to ensure the cantilever is clamped securely and to provide additional data points for uncertainty analysis.

For silicon cantilevers only, the mechanical loss is also found as a function of temperature. The cryostat is cooled down to ˜8K using liquid nitrogen and liquid helium. The mechanical loss of the cantilever is then measured as a function of frequency for three trials at 8K. After completing the three measurement sets, heaters attached to the clamping block warm the cantilever to the next measurement temperature. Upon stabilizing at the next measurement temperature, the entire loss measurement process is repeated. For measurements from
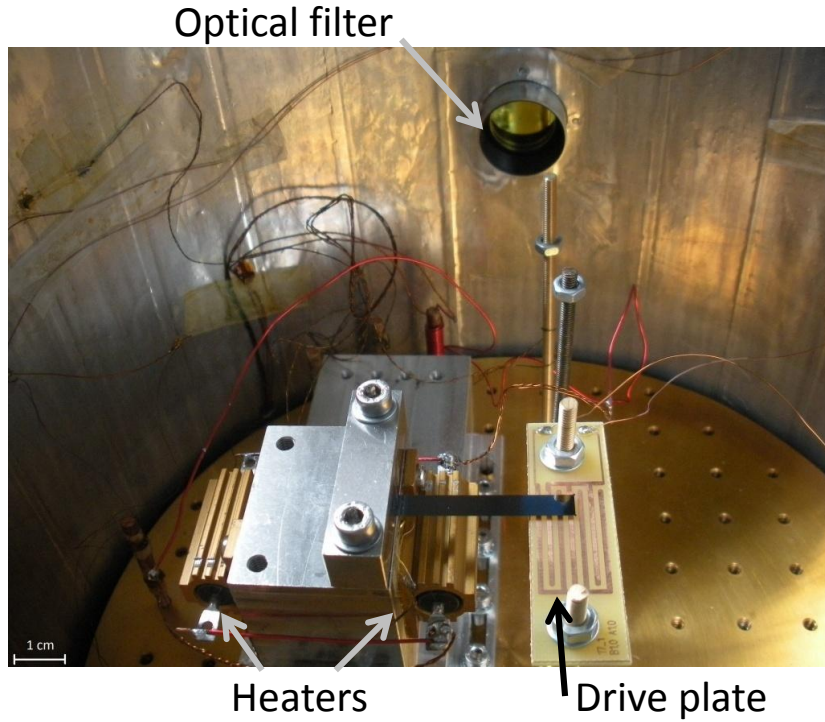
Figure 3: Cantilever clamped into a cryostat clamping block. Heaters on both sides of the clamping block regulate the clamp and cantilever temeprature.

$8-20$K, the temperature is increased in incrememts of 1K, and the temperature step sizes increase as the temperature of the system increases. Mechanical loss measurements are completed from 8 K to 295 K.

Measurements are not performed for silica as a function of temperature because silica is not a thermally conductive material and the temperature at the end of the cantilever may not be the same as the cantilever's clamped end. The cantilever temperature would add a significant uncertainty to loss measurements as a function of temperature. Additionally, silica's broad mechanical loss peak near 40K means low-temperature measurements are not beneficial for finding low mechanical losses.

After an uncoated cantilever is analyzed, the cantilever is sent to CISRO or ATFilms to receive a coating via the desired deposition technique (IBD, HWCVD, plasma-enhanced chemical vapor deposition (PECVD), etc.). All coatings measured through this project were deposited using ion beam sputtering for deposition. Once the cantilever is returned with a coating, the entire mechanical loss measurement process previously performed on the uncoated cantilever is repeated. The uncoated and coated mechanical loss measurements can then be compared and used to determine the mechanical loss of the coating.

6 Experimental Condition Control

6.1 Cryostat

The HDL-10 cryostat from IR Labs, Inc. is used for experimental condition control. The HDL-10 model uses multiple layers of shielding foil to insulate the system for regular operation at temperatures as low as 2K. HDL-10 cryostats contain two dewars for cryogenic cooling; one dewar holds liquid nitrogen and the second dewar contains liquid helium. The cryostat contains two optical filters on opposite sides of the experimental space for passing a laser beam across and analyzing the excitation amplitude of the cantilever. The clamp in the experimental space is attached to a base plate that is directly cooled by the helium space. The experimental cryostat space is located on the bottom of the cryostat; as such, evacuation of the nitrogen and helium spaces, shutdown of the pressure pumps, and manual flipping of the cryostat must be performed before the experimental sample can be accessed.

6.1.1 Vacuum pressure

To regulate the pressure conditions inside the cryostat, two different pumps are used in unison for atmospheric evacuation as seen in Fig. 4.
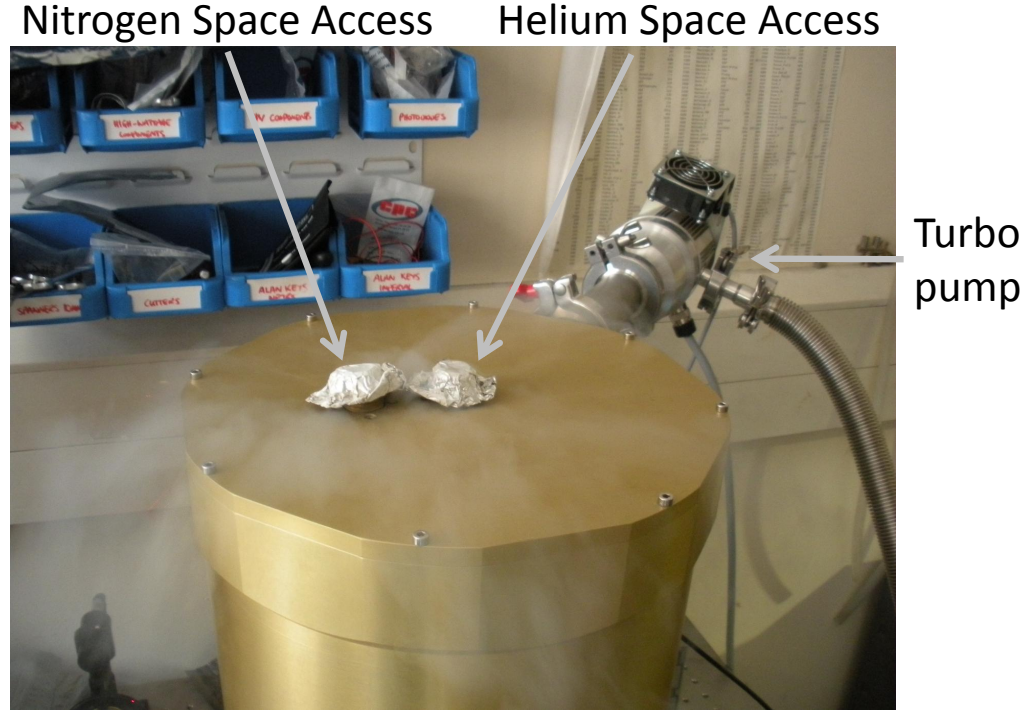

Figure 4: Pump system for cryostat pressure control. The turbo pump connects directly to the cryostat and prevents air particulates from entering, while a backing pump (not shown) connected via the large tube continues to evacuate the cryostat space.

A backing pump is first turned on to bring the cryostat from atmospheric pressure down to ~1×10^{-3} mbar. After the backing pump has ran for several minutes, a turbo pump is turned on to further reduce the pressure to ~1×10^{-6} mbar. The turbo pump fan oscillates at $1350\,Hz$ and prevents any air particles from returning into the cryostat.

6.1.2 Temperature regulation

Liquid nitrogen and helium are transferred from storage tanks as shown in Fig. 5 to nitrogen and helium spaces located inside the cryostat for achieving near-absolute zero temperatures.

Nitrogen Tank   Helium Tank

Figure 5: Liquid nitrogen and helium storage tanks. Liquid helium is a limited natural resource, so nitrogen is first used to cool the cryostats to minimize helium evaporation.

When cooling from room temperature, both the helium and nitrogen spaces are filled with liquid nitrogen to bring the entire cryostat down to ˜ 78 K. After the cryostat has reached equilibrium, the nitrogen in the helium space is removed and liquid helium is transferred into the helium space. Upon reaching thermal equilibrium at˜8K, the temperature of the clamp and cantilever can be

controlled using the clamp heaters (see Fig. 2).

7   Mechanical Loss Measurement Method

Mechanical loss measurements can be performed on the cantilever sample after preparing the desired experimental conditions. The cantilever is physically excited by a high-voltage drive plate resting below the sample (see Fig. 2). The drive plate is driven at any desired frequency, which in turn excites movement in the cantilever at the same frequency. Most frequencies of excitation will cause little vibration, but the cantilever has characteristic vibrational modes that can be calculated using[11]:

$$f_n = \frac{\alpha_n^2 t}{4\pi\sqrt{3}L^2} \left(\frac{\rho}{Y}\right)^{1/2} \tag{5}$$

where ρ is the cantilever density, Y is the cantilever's Young's modulus, L is the cantilever length, t is the cantilever thickness, and α_n is given for increasing values of n as

$$\alpha_n = 1.875, 4.694, 7.855, 10.996, \frac{\pi}{2}\left(2n-1\right), ... , \qquad n = 1, 2, 3, 4, 5...$$

After calculating the expected resonant frequencies, the actual resonant frequencies must be found experimentally. Imperfections in the sample, non-constant sample density, and uncertainties in the constants used to find the resonant frequencies will result in each theoretical resonant mode to be accurate within $\pm 5\%$. Upon finding the resonant modes, the cantilever excitation at these modes can be used in two ways to find the sample's mechanical loss.

7.1 FWHM Technique

For the FWHM analysis technique, the cantilever is excited with a drive plate through an entire excitation mode. The mechanical loss is found by measuring the full width at half maximum of the amplitude curve, measuring the frequency of the excitation mode, and using the frequency definition of the mechanical loss from equation (4), where

$$\phi = \frac{\Delta f}{f_0} \; .$$

This method of mechanical loss measurement is useful for taking one large scan across the entire frequency spectrum of a sample's excitation and measuring all of the excitation mode mechanical losses with one set of data. However, this method is not time-effective, as the modes are generally hundreds to thousands of hertz apart in the frequency spectrum. The FWHM technique can also be difficult to perform accurately due to asymmetrical resonant peaks.

7.2 Ringdown Technique

The second mechanical loss measurement technique involves exciting a resonant mode in a cantilever and removing the excitation once the cantilever has reached a max amplitude as shown in Fig. 6.
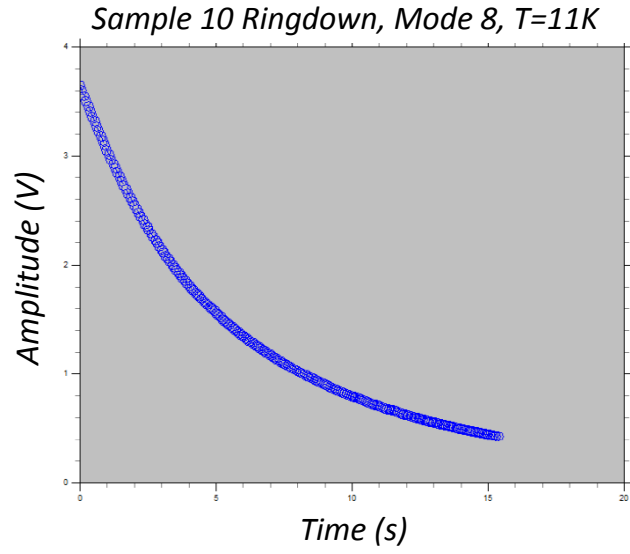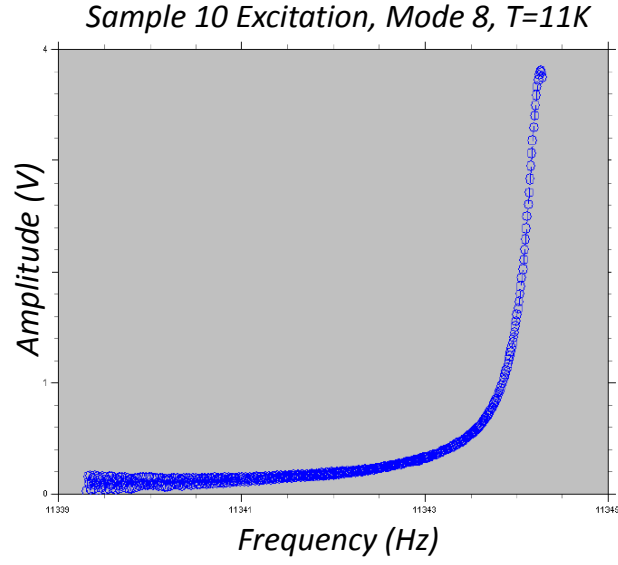
Figure 6: Amplitude excitation of a cantilever and subsequent amplitude decay resulting from the excitation removal.

The amplitude of the cantilever's vibration will exponentially decay with time due to loss mechanisms within the sample; with this in mind, the me-

chanical loss should be attainable through some analysis of the cantilever's de-excitation. The amplitude decay of a cantilever is described by

$$A(t) = A_0 e^{-\frac{t}{\tau}} \tag{6}$$

where τ is related to the mechanical loss with

$$\tau = \frac{1}{\pi f_0 \phi}$$

where f_0 is the resonant frequency and ϕ is the mechanical loss of the cantilever. For all mechanical loss measurements made in this paper, a ring-down technique was used to shorten data collection times.

8   Calculating the Coating Mechanical Loss

After analyzing a cantilever sample with and without a coating, the mechanical loss of the coating alone can be found by taking the difference of the two values and multiplying by an additional factor as such[12]:

$$\phi_{coating} = \frac{Y_s t_s}{3 Y_c t_c} \left[\phi(f_0)_{coated} - \phi(f_0)_{uncoated} \right] \tag{7}$$

where Y_s and Y_c are the Young's modulus of the substrate and coating, t_s and t_c are the thickness of the substrate and coating, and ϕ is the mechanical loss. The scaling factor containing the thicknesses and Young's moduli are necessary for a correct coating mechanical loss value because the cantilever itself stores more energy in the amplitude excitation process than the coating does.

For multilayer coatings, the mechanical loss of each individual material in the coating can also be calculated. Given a total coating mechanical loss, the individual coating losses are determined using[12]

$$Y_{coating}t_{coating}\phi_{coating} = Y_{l1}t_{l1}\phi_{l1} + Y_{l2}t_{l2}\phi_{l2} \tag{8}$$

where Y is the Young's modulus, t is the thickness, ϕ is the mechanical loss, and $l1$ and $l2$ are the the different layer materials. Thus, one of the layer's mechanical losses must be known to calculate the other layer's loss. Silica's coating loss has been chosen to be $\phi = 1 \times 10^{-4}$ for previous layer calculations[7] but has also been calculated to be 1.76×10^{-6} in experimentation with silica rods[13]. For the amorphous silicon / silica bilayer coating calculations in sec. 9.1, the mechanical loss of amorphous silicon is taken to be 5×10^{-5}.

8.1 Uncertainty in Coating Loss

The uncertainty in the total coating mechanical loss is found using a differential approximation technique. In general, the uncertainty for a calculated value $f(x_i)$ due to each variable x_i can be found using

$$\Delta f(x_i) = \sum_i \frac{df}{dx_i} \Delta x_i \tag{9}$$

where Δx_i is the uncertainty for each value x_i used to calculate $f(x_i)$. When calculating the uncertainty in a coating's mechanical loss, the two most significant sources of uncertainty are the mechanical losses of the coated and uncoated samples and the Young's modulus of the coating; other uncertainties are generally negligible for calculating the total coating loss uncertainty. Using eqn.(9) with the coating loss function (eqn.(7)), we can find that the coating's uncertainty is found using

$$\Delta\phi_{coating} = \frac{Y_s t_s}{3 Y_c t_c} \left[\Delta\phi_{coated} - \Delta\phi_{uncoated}\right] + \frac{Y_s t_s}{3 Y_c^2 t_c} \left[\phi_{coated} - \phi_{uncoated}\right] \Delta Y_c \; .$$

(10)

All that remains to find $\Delta\phi_{coating}$ is to find the uncertainties in the coated and uncoated losses and the coating's Young's modulus. For a loss measurement at any one frequency and/or temperature, the uncoated or coated loss uncertainty is determined by calculating the standard deviation of the three measured loss values produced from the sample clamping that has the *lowest* measured loss value. The data set with the lowest mechanical loss values is chosen because artificially low mechanical losses are more difficult to measure than artificially high mechanical losses (that is, the low mechanical losses can be considered more accurate than abnormally high mechanical losses). To find the uncertainty of a coating's Young's modulus, a weighted average of each material's Young's modulus uncertainty is used as such:

$$\Delta Y_c = \frac{\Delta Y_{l1} t_{l1} + \Delta Y_{l2} t_{l2}}{t_{l1} + t_{l2}} \; .$$

While the uncertainty in the substrate Young's modulus is generally neglible, the uncertainty for a coating's Young's modulus is approximately $\pm 10\%$ of the measured Young's modulus[14].

22

Part III

Results

9   Amporphous Silicon/Silica Bilayer Coating

Fig. 7 displays the mechanical losses calculated for Sample 16, a bilayer coating composed of 112 nm of amorphous silicon and 267 nm of amorphous silica on a silica cantilever. The coating layers were deposited using ion-beam sputtering, and the sample underwent no annealing prior to experimentation. Measurements were only completed at room temperature.
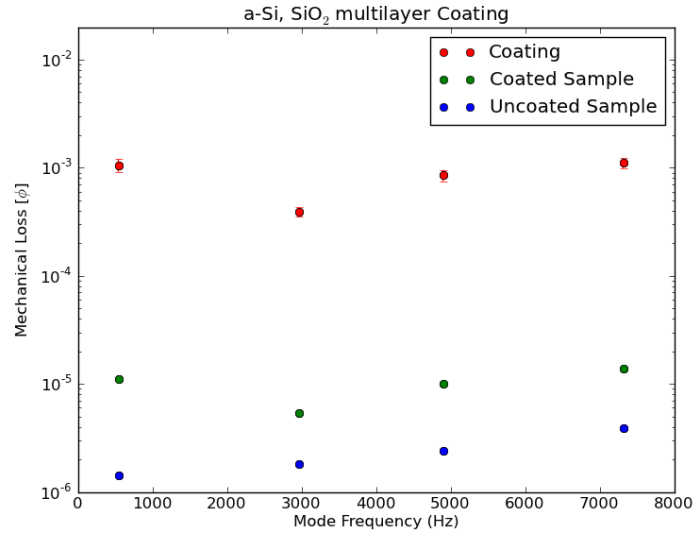

Figure 7: Mechanical loss measurement results for the amorphous silicon / silica bilayer coating at room temperature.

9.1 Bilayer and Individual Layer Losses for Amorphous Silicon

After measuring Sample 16's coating loss, the mechanical loss of the amorphous silicon material alone was calculated using equation (8) and by assuming amorphous silica's mechanical loss is $\phi_{SiO_2} = 5 \times 10^{-5}$. The mechanical loss of amorphous silicon as calculated from sample 16 is compared with the mechanical loss experimentally measured for a single layer of amorphous silicon deposited on a silica cantilever in Fig. 8.
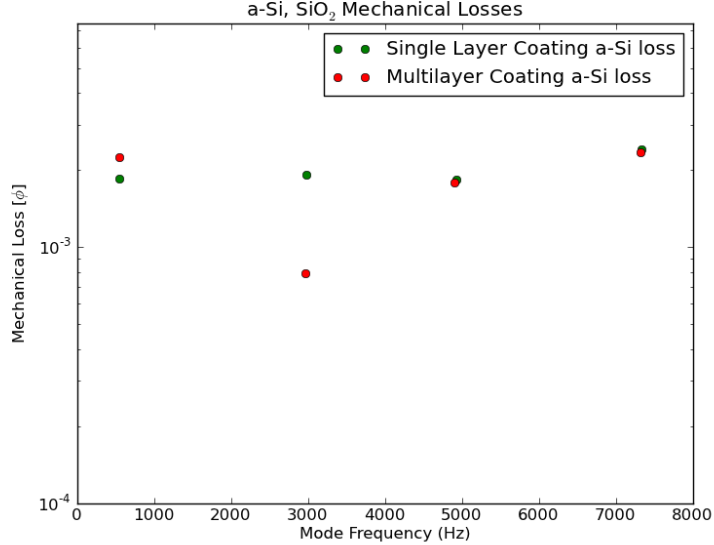

Figure 8: A comparison of amorphous silicon's mechanical loss in a bilayer configuration with amorphous silica and amorphous silicon's mechanical loss alone as the single coating material.

10   Single Layer Amorphous Silicon Coating

The coating loss results in Figs. 9 and 10 were measured from Sample 10, an amorphous silicon coating on a crystalline silicon cantilever annealed at $450°C$,

and Sample 16-12, an uncoated silicon cantilever annealed at $450°C$. The silicon cantilevers for Sample 10 and Sample 16-12 were not produced from the same silicon wafer. Figs. 9 and 10 display the measurements made on the sample's fourth and fifth natural resonant modes, respectively. The frequency of excitation for the fourth and fifth modes was $f_4 = 2738\,Hz$ and $f_5 = 4532\,Hz$ at $T = 15K$. Fig. 11 plots the coating mechanical losses from the foruth and fifth modes on the same graph for measurement comparison.
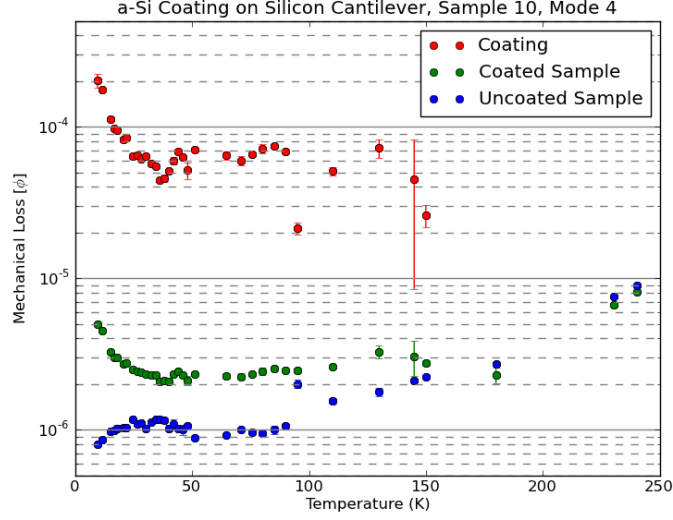

Figure 9: Sample 10's amorphous silicon coating loss as a function of temperature for the fourth resonant mode.
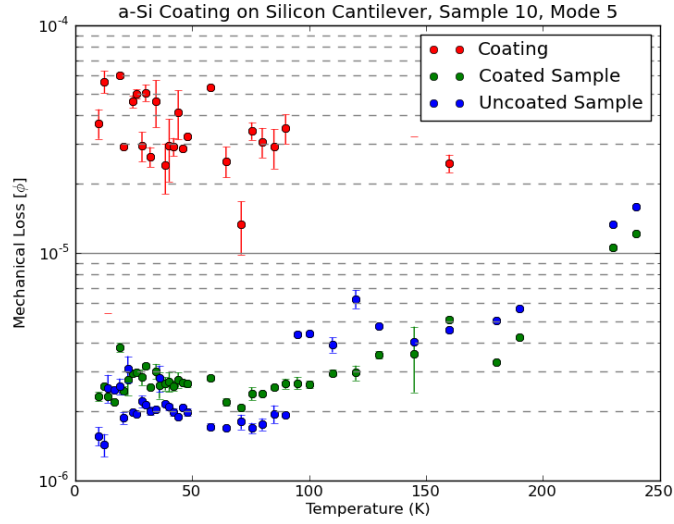
Figure 10: Sample 10's amorphous silicon coating loss as a function of temperature for the fifth resonant mode.
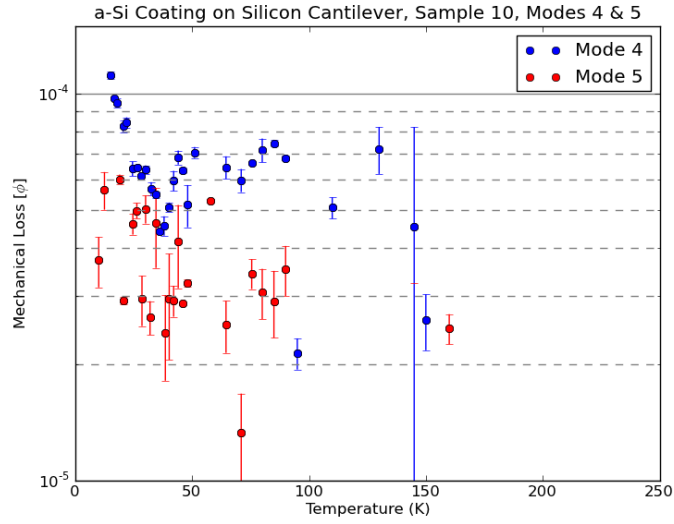

Figure 11: Coating mechanical losses of modes 4 and 5 for Sample 10.

Part IV

Discussion

11   Amorphous Silicon / Silica Bilayer Coating

Let us first consider the uncoated and coated mechanical losses used to calculate the coating loss. An important trend in the measured mechanical losses in Fig. 7 is the mechanical loss increase resulting from coating the sample. Since the overall thickness of the sample increases, more energy should be dissipated in the entire sample and result in a larger mechancal loss from our definition in equation (3); as such, the increase in mechanical loss after adding a coating makes physical sense. Additionally, the coating placed on the silica cantilever increases the sample's mechanical loss by nearly an order of magnitude for each measured resonant mode. Although the large loss increase indicates we may see a larger coating loss than desired, a large coating loss compared to all other losses in the system will result in a more accurate coating loss calculation. If the difference in coated and uncoated mechanical losses is too small, loss uncertainties due to outside factors such as clamping loss or thermoelastic loss can make finding the coating loss more challenging.

For the amorphous silicon / silica bilayer coating loss, mechanical loss measurements ranged from $\phi = 3.9 \pm 0.4 \times 10^{-4}$ to $\phi = 1.1 \pm 0.1 \times 10^{-3}$. The lowest mechanical loss measured for the coating is approximately twice the minimum mechanical losses measured for the gravitational interferometer-standard titanium-doped tantala / silica bilayer coating[7]. Considering only mechanical loss magnitudes, the measurements completed for Sample 16's coating would indicate that the titania-doped tantala / silica multilayer coating is a better candidate for gravitational interferometery, but Sample 16's optical properties

would have to be analyzed to be sure which coating is more beneficial for test mass coating.

11.1 Amorphous Silicon Loss Calculated From Coating Loss

The coating losses measured for Sample 16 were used with equation (8) to find the mechanical loss of amorphous silicon alone. Fig. 8 compares the loss measurements for sample 16's amorphous silicon layer to a single layer amorphous silicon coating previously measured at the University of Glasgow. The higher frequency modes have consistent mechanical loss values, indicating that equation (8) is reasonably accurate. The lower frequency modes do not match as well for our samples. Inconsistency in the multilayer-calculated loss and the single layer experimentally measured loss is more common than consistent results; this inconsistency is possibly a result of surface interactions between the different layers in the bilayer coating, but solid experimental evidence for a cause is yet to be found.

Using the silica mechanical loss value of $\phi_{SiO_2} = 5 \times 10^{-5}$, the lowest resulting loss for amorphous silicon alone was $\phi_{a-Si} = 7.8 \times 10^{-4}$. Comparing the two mechanical losses, the amorphous silicon loss at room temperature is over an order of magnitude larger than the silica loss; as such, Sample 10's mechanical loss is mostly limited by the amorphous silicon layer at room temperature. To improve the coating's mechanical loss, future work should target the amorphous silicon material in multilayer coatings for minimizing mechanical loss. Another possibility to improving this coating's loss could be to analyze the coating somewhere between 100K (where silica's 40K mechanical loss peak ends) and 150K (where the thermoelastic loss begins to limit amorhpous silicon's mechanical loss) and see if the mechanical loss measurements improve.

12   Single Layer Amorphous Silicon Coating

The uncoated and coated mechanical loss measurements for Sample 10 are much closer in magnitude than those observed for Sample 16. The closeness in uncoated and coated mechanical loss can be attributed to a combination of the coating material being similar to the cantilever (amorphous silicon and crystalline silicon) and the generally low mechanical loss of amorphous silicon at low temperatures. The small change in the sample's loss due to the addition of a coating indicates the coating's loss could be low, but uncertainties due to additional loss factors will increase. For example, as the temperature rises, the coated mechanical loss becomes smaller than the uncoated mechanical loss in Figs. 9 and 10, an unphysical result that can be attributed to an increase in thermoelastic loss and thermoelastic loss uncertainties as the system temperature increases[9].

The mechanical loss curves for the uncoated and coated samples in mode 4 show very different behavior in the temperature range from 8K to 25K. For an identical sample with an added coating, the mechanical loss curves would most commonly share the same peaks or the coated sample would develop new peaks due to mechanical loss peaks characteristic to the coating material; opposing curve orientations are generally not expected. The opposing curve orientations for mode 4 are most likely an artifact resulting from how the coated and/or uncoated samples were clamped. The cooling process can cause the clamp to tighten or loosen from thermal-related material density fluctuations, and as the clamp warms up towards room temperature the mechanical loss curve can change due to the same effect.

The mechanical losses for modes 4 and 5 of the amorphous silicon coating agree within an order of magnitude as seen in Fig. 11. Contrary to the loss as a function of frequency for Sample 16, Sample 10's mechanical loss is lower for the

higher frequency mode. More modes would need to be analyzed to determine if this trend is common across all modes or if the lower loss for mode 5 is a product of a lower clamping loss.

Sample 10's coating mechanical losses were found to range from $\phi_{coating} = 1.3 \pm 0.35 \times 10^{-5}$ to $\phi_{coating} = 6.2 \pm 0.16 \times 10^{-5}$. The losses measured for Sample 16's amorphous silicon coating deposited with ion beam deposition are on the same order of magnitude as the losses previously made on coatings deposited with HWCVD and PECVD at the Washington D.C. Naval Research Laboratory[8]. Additionally, the lowest measured loss for Sample 10's coating is lower than the loss measurements performed on amorphous silicon films deposited through HWCVD with any H_2 dilution. Hydrogenated amorphous silicon film mechanical losses (similar to those seen in solar panels[15]) reside lower than Sample 10's amorphous silicon coating loss by nearly two orders of magnitude.

Part V

Conclusion

Room temperature measurements for the mechanical loss of Sample 16's amorphous silicon-amorphous silica bilayer coating resulted in a lowest mechanical loss measurement of $\phi_{coating} = 3.9 \pm 0.4 \times 10^{-5}$ and an upper bound of $\phi_{coating} = 1.1 \pm 0.1 \times 10^{-4}$. The lowest loss measured is approximately twice the measured mechanical loss for the interferometer standard titania-doped tantala / silica multilayer coating and only slightly larger than single layer titania-doped tantala[7]. Assuming that the mechanical loss of the amorphous silica layer in Sample 10 was $\phi_{SiO_2} = 5 \times 10^{-5}$, the lowest mechanical loss calculated

for the amorphous silicon layer at room temperature was $\phi_{a-Si} = 7.8 \times 10^{-4}$. The order of magnitude difference in the layer losses indicates that amorphous silicon's mechanical loss is the major contributor to the coating mechanical loss at room temperature.

Mechanical loss measurements for Sample 10's single layer amorphous silicon coating resulted in mechanical losses between $\phi_{coating} = 1.3 \pm 0.35 \times 10^{-5}$ ($T = $ 71K) and $\phi_{coating} = 6.2 \pm 0.16 \times 10^{-5}$ ($T = $ 19K). The mechanical loss of amorphous silicon in the $8-50$K range is much lower than the room temperature losses previously measured at University of Glasgow, indicating that amorphous silicon would be more beneficial for use in cryogenically cooled interferometers than the room-temperature interferometers commonly utilized.

Experimentation performed on Sample 16 and Sample 10 has left several opportunities for future work and follow-up. To acquire a more complete picture on the coatings' applicability to gravitational interferometery, the reflectance and optical absorption of Sample 16 and Sample 10 should be measured and compared to those seen in titania-doped tantala / silica multilayer coatings and titania-doped tantala single layer coatings. Further investigation into modeling surface interactions within multilayer coatings could also help answer why the a material's bilayer mechanical loss and single layer mechanical loss can be inconsistent. Possible solutions to the closeness of the coated and uncoated mechanical losses for Sample 10 should also be considered; in particular, the surface etching of silicon[16] could be a viable option to lowering the cantilever loss without varying the cantilever material. The Washington D.C. Naval Research Laboratory's low mechanical loss measurements for hydrogenated amorphous silicon also provide motivation for attempting to dope amorphous silicon in hopes of lowering a coating's loss much like titania-doped tantala.

Part VI

Acknowledgements

Part VII

Resources

References

[1] Hough, J., Rowan, S. The search for gravitational waves. Physics World. V.18 No.1 (January 2005): 37-41.

[2] Aasi, J., et al. Virgo data characterization and impact on gravitational wave searches. arXiv:1203.5613v1 [gr-qc] 26 Mar 2012.

[3] Cumming, A.V., et al., "Design and development of the advanced LIGO monolithic fused silica suspension." Classical Quantum Gravity 29 (2012).

[4] Martin, I. "Studies of materials for use in future gravitational wave detectors." Ph.D. thesis, University of Glasgow (2009).

[5] Harry, G., Gretarsson, A., Saulson, P., Kittelberger, S., et al., "Thermal noise in interferometric gravitational wave detectors due to dielectric optical coatings." Classical and Quantum Gravity 19 (2002) 897917.

[6] Martin, I., et al., Effect of heat treatment on mechanical dissipation in Ta_2O_5 coatings. Classical and Quantum Gravity 27 (2010).

[7] Harry, G., et. al., "Titania-doped Tantala / Silica Coataings for Gravitational Wave Detection." Classical and Quantum Gravity 24 (2006).

[8] Liu, X., et al., "Internal friction of amorphous and nanocrystalline silicon at low temperatures." Materials Science and Engineering A 442 (2006).

[9] Photiadis, D.M., et al., "Thermoelastic loss observed in a high Q mechnical oscillator." Physica B 316-317 (2002).

[10] Kuroda, K. "Status of LCGT." Classical and Quantum Gravity 27 (2010).

[11] McLachlan, N. M., "Theory of Vibrations." New York: Dover, 1952.

[12] Crooks, D. R. M., "Mechanical loss and its signficance in the test mass mirrors of gravitational wave detectors." Ph.D. thesis, University of Glasgow (2002).

[13] Penn, D., et al., "High Quality Factor Measured in Fused Silica." Review of Scientific Instruments V. 72 No. 29 (2001).

[14] Li, L., et al., "Simultaneous determination of the Youngs modulus and Poissons ratio in micro/nano materials." J. Micromech. Microeng. 19 (2009).

[15] Oh, J. Yang, J. et al., "Effects of TiO$_2$ nanopatterns on the performance of hydrogenated amorphous silicon thin-film solar cells." Thin Solid Films 520 (2012).

[16] Tabata, O. "Anisotropic Etching of Silicon in TMAH Solutions." Sensors and Materials V. 13 No. 5, 271-283 (2000).